73rd International Astronautical Congress (IAC), Paris, France, 18-22 September 2022.

IAC-22,B4,8,6,x72031

Design of the vision-based GNC subsystem of Hera's Milani mission

Felice Piccolo[1], Antonio Rizza[2], Mattia Pugliatti[3], Vittorio Franzese[4], Claudio Bottiglieri[5], Carmine Giordano[6], Fabio Ferrari[7], Francesco Topputo[8]

Milani is a 6U CubeSat that will be released by ESA's Hera spacecraft near the binary asteroid system 65803 Didymos. Its scientific objectives are to acquire high-resolution images of the two asteroids and characterize the dust environment in their vicinity. This work describes in detail Milani's Guidance, Navigation & Control subsystem. Its main tasks are to compute a primary pointing direction and estimate the state of the spacecraft with respect to the asteroid system. To this aim, an onboard Extended Kalman Filter has been implemented. It uses image processing observables and lidar measurements. Furthermore, different pointing strategies have been introduced to increase the robustness of the attitude guidance. The GNC can select the appropriate mode autonomously, depending on the available data. The design has been validated through extensive analyses that covered nominal and off-nominal scenarios. The most significant results are reported in this work.

1 Introduction

The Asteroid Impact & Deflection Assessment (AIDA) mission is the first full-scale test of a planetary defense mission [1]. Its objective is to assess the deflection capability of a kinetic impactor on hazardous near-Earth objects. AIDA is an ESA-NASA collaboration that will send two spacecraft to the binary asteroid 65803 Didymos. First, NASA's Double Asteroid Redirection Test (DART) mission will impact the secondary asteroid of the system, Dimorphos, to alter its orbit [2]. Then, ESA's Hera spacecraft will rendezvous with the binary system to characterize it following DART's impact [3]. In proximity of the target, Hera will release two 6U CubeSats: Milani and Juventas. Milani will perform hyperspectral imaging of the asteroids' surface and will characterize the dust environment around the system [4]. Juventas will carry a low-frequency radar to study the internal structure of the asteroids [5]. The CubeSats will communicate with Hera using an Inter-Satellite Link (ISL), which will be demonstrated for the first time in deep space. Milani and Juventas will operate indipendently, but they will rely on the mothercraft to communicate with Earth.

This work describes Milani's vision-based Guidance, Navigation & Control (GNC) subsystem. It is characterized by semi-autonomous capabilities enabled by innovative Image Processing (IP) and autonomous navigation components, paired with traditional guidance and control methods. The main task of the GNC subsystem is to provide the pointing direction to the desired target, with the capability to switch between Didymos (D1), Dimorphos (D2), and Hera. Even if the nominal orbit determination of the spacecraft will be performed with a classical ground-based approach, the GNC includes an onboard Extended Kalman Filter (EKF) that autonomously estimates the spacecraft state using IP observables and range measurements from a lidar sensor. The onboard EKF will be employed both for pointing purposes and as part of an autonomous optical navigation experiment. The GNC subsystem has been validated through extensive analyses in nominal and off-nominal conditions.

This paper is framed in the context of a series of works describing different aspects of the Milani mission. An overview of the mission and a high-level description of the IP and GNC subsystems is given in [6]. A more detailed description of the IP algorithm can be found in [7] and [8], while the updated mission analysis is discussed in [9]. The interested reader can also find a summary of the preliminary mission design in [4] and [10], which refer

[1]PhD Student, Department of Aerospace Science and Technology, Politecnico di Milano, Via La Masa 34, 20156, Milano, Italy; felice.piccolo@polimi.it
[2]PhD Student, Department of Aerospace Science and Technology, Politecnico di Milano, Via La Masa 34, 20156, Milano, Italy, antonio.rizza@polimi.it
[3]PhD Student, Department of Aerospace Science and Technology, Politecnico di Milano, Via La Masa 34, 20156, Milano, Italy, mattia.pugliatti@polimi.it
[4]PostDoc Researcher, Department of Aerospace Science and Technology, Politecnico di Milano, Via La Masa 34, 20156, Milano, Italy, vittorio.franzese@polimi.it
[5]Research Assistant, Department of Aerospace Science and Technology, Politecnico di Milano, Via La Masa 34, 20156, Milano, Italy, claudio.bottiglieri@polimi.it
[6]PostDoc Researcher, Department of Aerospace Science and Technology, Politecnico di Milano, Via La Masa 34, 20156, Milano, Italy, carmine.giordano@polimi.it
[7]PostDoc Researcher, University of Bern, Physics Institute, Gesellschaftsstrasse 6, 3012 Bern, Switzerland fabio1.ferrari@polimi.it
[8]Full Professor, Department of Aerospace Science and Technology, Politecnico di Milano, Via La Masa 34, 20156, Milano, Italy, francesco.topputo@polimi.it

to the phase 0 and phase A of the mission, respectively.

The remainder of the paper is organized as follows. Sections 2 and 3 give a brief overview of the Milani mission and of the IP algorithm, respectively. Then, the GNC design is detailed in Section 4. In Section 5 the analyses conducted on the GNC are presented and the main results are discussed. To conclude, Section 6 gives the final remarks.

2 Mission overview

Milani will be released by Hera in proximity of Didymos after an initial characterization phase. It will carry two scientific payloads: ASPECT, a hyperspectral imager [11], and VISTA, a thermogravimeter sensor [12]. Furthermore, the platform will host the ISL radio and a suite of sensors for navigation and attitude determination. The latter include a star tracker, an inertial measurement unit (IMU), a lidar, and a navigation camera (NavCam). The main scientific objectives of the mission are: 1) to obtain high-resolution images of the asteroid's surfaces, with particular focus on Dimorphos and on DART's impact crater; 2) to characterize the dust environment around the binary asteroid. From a technological point of view, the main goals are: 1) to validate autonomous navigation algorithms; 2) to test the ISL communication with Hera.

The mission is divided into different phases that are designed to progressively achieve its objectives. After its release, the spacecraft will enter a Far Range Phase (FRP), where it will perform the global mapping of both asteroids at a resolution of 2 m/pixel. During FRP, Milani will move along symmetric hyperbolic arcs at a distance of 8 to 14 km from the main asteroid. The duration of FRP arcs alternates between 3 and 4 days, for a total of approximately 21 days. Next, a Close Range Phase (CRP) will follow, which is characterized by a more complicated design, conceived to meet more challenging requirements. During CRP, the spacecraft will perform the global mapping of the secondary asteroid, Dimorphos, at 1 m/pixel. Furthermore, it will acquire images of DART's impact crater at 50 cm/pixel resolution. The latter is the most challenging scientific objective, and it has been the main driver for the trajectory design. Most of the CRP arcs have a 7-days duration to allow sufficient operational time to compute and command trajectory correction maneuvers from ground. These are necessary to reduce trajectory dispersion, since the spacecraft gets significantly closer to the system. The CRP will last for a total of approximately 35 days. Its trajectory is characterized by asymmetric hyperbolic arcs that cover a range of 2 to 21 km from Didymos. More details on the mission analysis of Milani, and in particular of the CRP design, can be found in [9]. After CRP, Milani will enter an experimental phase in which it will transfer to a terminator orbit around the primary asteroid. Finally, it will either attempt a landing on Dimorphos or be injected into a safe heliocentric orbit. The nominal trajectories for the FRP and CRP are represented in Fig. 1. They are shown in the DidymosECLIPJ2000 reference frame, which is a quasi-inertial frame defined as follows: the origin is the barycenter of the Didymos system, the x-axis points towards the vernal equinox, the z-axis is perpendicular to the ecliptic plane, and the y-axis completes the right-handed set.

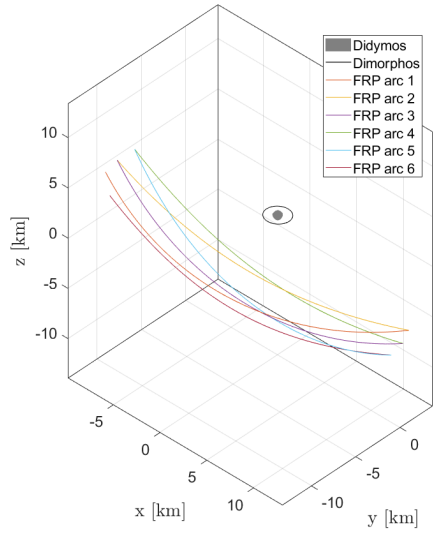

(a) FRP

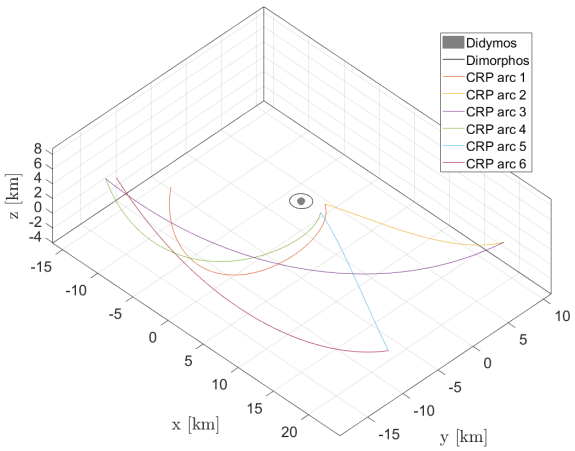

(b) CRP

Fig. 1: Nominal trajectory for FRP and CRP. The legends report the nomenclature used for the different arcs.

3 Image Processing

Given the strict connection between the GNC and the IP, a brief description of the latter is given in this section. More details can be found in [7] and [8]. The task of the IP algorithm is to process incoming NavCam images to extract information about the asteroids. In particular, D1 is used for navigation purposes since it is expected to be more regular than D2 and it is always visible. However, D2 is the the main scientific target of the mission, so the IP must be able to identify it for pointing purposes.

The IP pipeline is divided in two main blocks: the 'Blobs Characterization' and the 'Observables Extraction'. The former distinguishes D1 from D2 in the image and performs a simple blob analysis, while the latter extracts high-level observables. The most important quantity is the Center of Figure (CoF) of D1, that is used by the GNC for both pointing and navigation. The CoF is the estimation of the location of the Center of Mass (CoM) of D1 in the image. The IP also estimates the phase angle (Sun-asteroid-spacecraft angle) and range from D1 and the CoF of D2, when it is visible. Three alternative algorithms are available to estimate the CoF of D1, that are called COB (Center Of Brightness), WCOB (Weighted Center Of Brightness) and SSWCOB (Sun Sensor Weighted Center Of Brightness). The COB is the simplest one, in which the CoF is simply estimated as the centroid of the largest blob of pixels in the image. The WCOB and SSWCOB are data-driven methods that improve the CoF estimation by applying a correction that depends on the phase angle and range. In the WCOB method the phase angle and the Sun direction are estimated autonomously by the IP algorithm, while the SSWCOB relies on data provided by the Sun sensors, which are typically more accurate than those estimated directly from the image.

4 GNC design

Milani's GNC subsystem is in charge of providing a primary pointing solution to the Attitude Determination and Control Subsystem (ADCS). During most of the mission, the primary pointing is intended as the direction in which the navigation camera has to be pointed. However, in some cases, other conditions could be needed. For example, it may be desired to direct one of the ISL antennas towards Hera. Once the primary pointing direction is fixed, the spacecraft can roll about that axis to satisfy other constraints like star tracker coverage and power generation. This additional degree of freedom is managed by the ADCS. In addition, the GNC produces an estimate of the spacecraft state (position and velocity) with respect to Didymos' barycenter. The GNC and ADCS subsystems form the attitude and orbit control system (AOCS). Its architecture is reported in Fig. 2, which illustrates the connections of the GNC with the rest of the system. The GNC and ADCS are deeply interrelated as they continuously exchange data. Furthermore, the GNC is directly connected to the lidar and the NavCam.

The GNC is composed of five main blocks, as illustrated in Fig. 2. The first one is a pre-processing block, in which some initial checks are performed on the input variables to ensure their validity. These include a freshness check to make sure that the variables have been updated recently enough, and a check on their values to verify that they are in the expected range. Then, a state machine determines the appropriate operative modes. The navigation and guidance blocks compute the estimated spacecraft state and the desired pointing direction according to the selected operative mode. Finally, the health check block verifies the validity of the solutions. The main elements of the GNC subsystem are discussed in more detail in the following sections.

4.1 GNC modes

A set of operative modes is used to describe and regulate the functionality of the GNC subsystem. In particular, at high-level a GNC mode is defined to communicate the status of the GNC to the rest of the system. Then, a submode is associated to each of the navigation, guidance and EKF modules. The submodes determine the algorithms that are executed within each block. Tab. 1 reports the possible values of the GNC mode, together with a brief description for each of them. The navigation, guidance and EKF modes are instead discussed in the following sections.

4.2 State machine

The state machine determines the appropriate operative modes at every GNC execution. Each one of them is selected according to a specific truth table, which checks a series of logical conditions. The navigation, guidance and EKF submodes are first computed. Then, depending on their values, the GNC mode is determined. In all cases, a hierarchical approach is followed. The default mode is always the simplest one and, if the necessary conditions are met, the system switches to more complex modes. The highest reachable mode can be limited by a set of input variables. The only exception to this scheme is *Asteroid Search*. Since it is intended as a contingency strategy, the GNC cannot transition to this

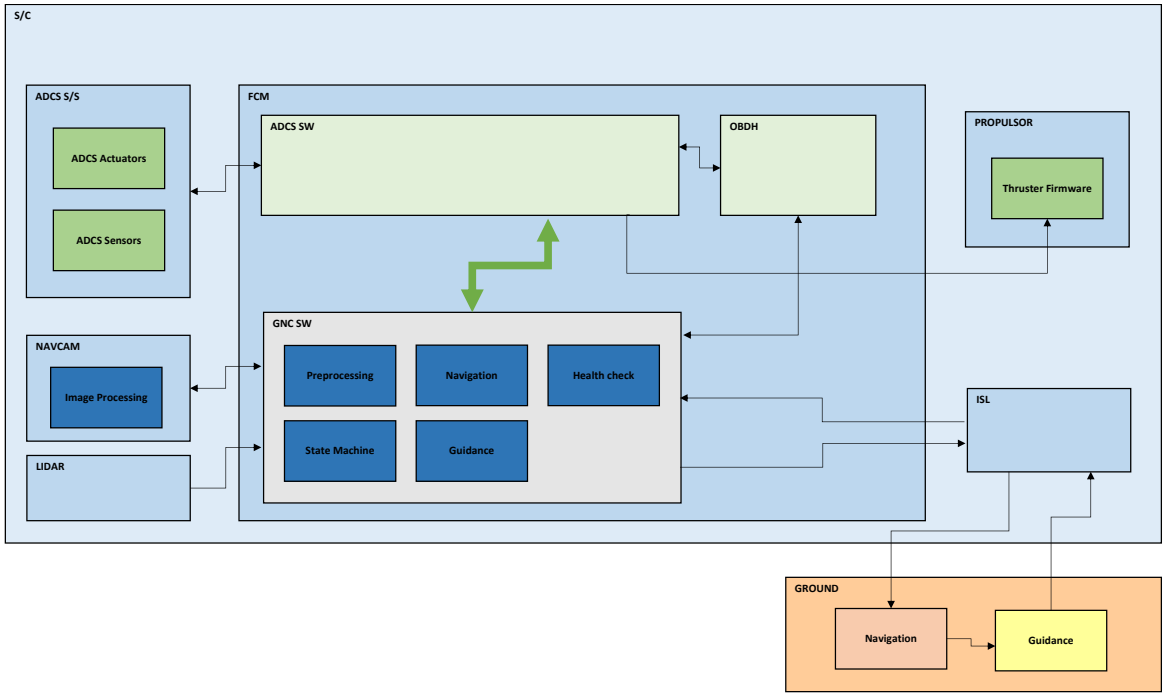

Fig. 2: Architecture of the AOCS system.

Tab. 1: GNC modes

GNC mode	Description
Drift	Issue detected both in Navigation and Guidance. Neither the navigation nor the guidance solution is considered reliable.
Nav. Only	Guidance section not working as expected. Guidance solution cannot be considered reliable. Best navigation solution is targeted.
Gui. Only	Navigation section not working as expected. Navigation solution cannot be considered reliable. Best guidance solution is targeted.
Nominal	Both navigation and guidance solutions are successfully computed. Best solutions are targeted.
Asteroid Search	Navigation based on ephemerides (if possible), guidance submode set to re-acquire the target.

mode autonomously, but it can only be enabled from ground.

4.3 Navigation

The navigation module estimates the state of the spacecraft with respect to Didymos' barycenter. Three navigation submodes are available: *Nav. keep last*, *Nav. from Eph.*, and *Nav. from EKF*. In *Nav. keep last*, the navigation solution is not updated, thus the last solution produced is kept as output. *Nav. from Eph.* is based on the interpolation of ephemerides data provided from ground. Ephemerides are stored onboard as a matrix of Chebyshev polynomials coefficients, which are then interpolated using their recursive formulation. The coefficients are associated with specific time bounds that indicate the limits within which the set is valid. Two sets of coefficients are stored on-board for Milani, which are referred to as nominal and standby. They store the coefficients for the current and the next trajectory arc, respectively. When a manoeuvre occurs, the coefficients used by the GNC are automatically updated. This strategy has a double purpose: first, it avoids the necessity of interpolating multiple trajectory arcs using a single set of coefficients, which would degrade the ephemerides accuracy; second, it provides robustness for contingency scenarios. Indeed, with this strategy a set of coefficient can be used to cover a longer time span. By propagating the ephemerides beyond the nominal duration of a trajectory arc, a rough estimation of the spacecraft poisition can be obtained even in case of a missed manoeuvre.

Nav. from EKF provides the solution computed by the onboard EKF. The latter relies on IP and lidar measurements to estimate the spacecraft state. The dynamic

model used in the EKF accounts for the gravitational effects of D1, D2 and the Sun, all treated as point masses, and for the Solar Radiation Pressure (SRP) using a simple cannonball model. The equations of motion are propagated using a Runge-Kutta 4 integrator. To account for uncertainties in the dynamics, residual accelerations and a fraction of the SRP are treated as Gauss-Markov processes with the properties given in Tab. 2.

The following operative modes are possible for the EKF, depending on the available inputs: *EKF keep last*, *Propagation only*, *Propagation + lidar*, *Propagation + IP*, *Propagation + lidar + IP*. In *EKF keep last*, the solution is not updated. In *Propagation only*, the state is propagated up to the current time, but no measurements are used. In the remaining modes, the state is propagated and the available measurements are used to correct the estimation. Specifically, the EKF uses the estimated CoF of D1 and the range measurement from the lidar. The other IP measurements have been discarded because they are less reliable. The IP algorithm is designed to work within a range of 3 to 23 km from the system. The lidar sensor, instead, produces measurements at a maximum range of 5.5 km, so it is used only during CRP.

It is assumed that measurements are affected by Gaussian random noise with 0 mean and standard deviation given in Tab. 3. The uncertainty used for the range measurement accounts for both the error due to the lidar sensor and the uncertainty on the shape of D1. The 0-mean Gaussian assumption is reasonable for the range measurement and for the WCOB and SSWCOB methods of the IP. For the simple COB method, instead, a bias in the CoF measurement is expected at high phase angles. However, the use of COB is foreseen only as a backup option in case of issues with the other IP methods, so the EKF is not designed to work with it for extended periods of time.

When IP measurements are available, a consistency check is performed on the EKF output. It has the objective to verify that the estimation error is consistent with the expected covariance matrix. The check is based on the Normalized Innovation Squared (NIS) of the CoF measurement:

$$n = (\boldsymbol{y} - \hat{\boldsymbol{y}})^{\mathrm{T}} (\mathrm{H}\bar{\mathrm{P}}\mathrm{H} + \mathrm{R})(\boldsymbol{y} - \hat{\boldsymbol{y}}) \tag{1}$$

where n is the NIS, $\boldsymbol{y}$ is the measurement, $\hat{\boldsymbol{y}}$ is the EKF reference measurement, H is the Jacobian of the measurement with respect to the state, $\bar{\mathrm{P}}$ is the time-updated covariance matrix of the state vector, and R is the covariance matrix of the measurement noise. Under the EKF's hypotheses, the NIS should follow a chi-squared probability distribution, with degrees of freedom equal to the number of measurements considered [13]. This assumption can be used to check how likely the current value of the residuals is. If it is highly unlikely, some of the hypotheses are probably being violated. The consistency check is based on the CoF measurement because it is the most reliable one. However, this choice makes the evaluation insensitive to errors in the camera boresight direction. To increase robustness against statistical fluctuations and possible measurement outliers, the consistency check relies on the sum of last three values of the NIS. This sum follows a chi-squared distribution with three times the number of degrees of freedom. Then, the cumulative distribution function of the sum is computed. If it is above a certain threshold, the EKF output is considered invalid.

A similar check is also performed for the lidar measurement, but it is used to confirm the validity of the measurement itself rather than the EKF solution. When new lidar measurements are produced, they are compared with the range currently estimated by the EKF. The NIS of each measurement is computed, and then its probability is evaluated by assuming a chi-squared distribution. If the measurement is highly unlikely, it is discarded. This check has been introduced mainly to reject spurious lidar measurements obtained when the lidar is pointing at D2 instead of D1.

4.4 Guidance

The guidance module computes the desired primary pointing direction. Five guidance submodes have been designed: *Gui. keep last*, *Reference*, *Tracking*, *Predicted*, and *Search Pattern*. As for the navigation module, *Gui. keep last* maintains the last solution computed. In *Reference*, guidance is obtained from ground-provided information, either by following a specified pointing profile or interpolating ephemerides data. In *Tracking*, IP data is used to bring the target to the center of the NavCam field of view (FOV). In particular, it uses the CoF estimation to compute the rotation needed to center the target. The target can be D1 or D2, if the latter can be distinguished from the main asteroid. While waiting for new IP data, a fixed inertial pointing direction is kept. *Predicted* combines the position estimated by the onboard EKF with the ephemerides of the target to compute the guidance solution. In this case, the target can be any body for which ephemerides are available on board. For example, this strategy can be used to point at D2 when the IP software is not able to recognise it in the image, or to point at specific features on the asteroids, like DART's impact crater. Finally, *Search Pattern* is a submode devised to search for the target in case it is lost from the NavCam FOV and the other strategies fail to recover it. It computes the primary pointing by

Tab. 2: Statistical properties of the residual acceleration and SRP. σ is the standard deviation of the white noise driving the Gauss–Markov process, τ is the autocorrelation time.

	σ	τ
Residual acceleration	$5 \times 10^{-9} m/s^2$	1 day
Solar Radiation Pressure	8% of SRP acceleration magnitude	1 day

Tab. 3: Standard deviations assumed for EKF measurements

Measurement	σ
Range	15 m
CoF - COB	40 px
CoF - WCOB	20 px
CoF - SSWCOB	15 px

following a predefined map stored onboard. The latter is defined relatively to the pointing direction at the beginning of the search. When the target is found, the guidance submode automatically switches to *Tracking*. The *Search Pattern* submode is available only when the GNC mode is set to *Asteroid Search*, therefore it cannot be activated autonomously, but it must be enabled from ground.

4.5 FDIR

Given the level of autonomy required by the GNC subsystem, the latter must be capable of identifying and responding to unexpected events. The FDIR (Fault Detection, Isolation and Recovery) strategy relies mainly on the preprocessing block and the state machine. Indeed, the first is in charge of detecting potential issues by checking the validity of the input variables. The second uses the results of these checks to select the suitable operative modes, adapting automatically in case of missing data or problems with other subsystems. Furthermore, the health check block is in charge of detecting possible issues in the GNC output. It verifies the validity of the navigation and guidance solutions and returns specific validity flags associated with them. The checks consist in verifying that the solutions are within the expected bounds and that the primary pointing direction is outside of a predefined Sun exclusion angle to avoid damage to the optical sensors. If issues with one or both solutions are detected for a certain number of consecutive GNC executions, the GNC mode is updated accordingly.

5 Results

Extensive analyses have been performed to validate the proposed GNC design. They focused mainly on two objectives. The first is to confirm that the GNC behaves as expected during nominal and off-nominal events, like attitude and orbital manoeuvres, sensor faults, missing input data, etc. The second is to assess the performance in terms of pointing and navigation accuracy. In particular, there are two main requirements on the GNC performance. One states that the pointing error during scientific acquisitions shall be below 0.5 deg, 1-sigma. The other requires that the GNC shall be able to reconstruct the spacecraft position with an error below 10% of the true range for 50% of the duration of each arc.

The analyses are divided into four categories, which are reported in Tab. 4. They have been conducted on both nominal and dispersed trajectories. The latter are trajectories that deviate from the nominal one according to the statistical uncertainty expected by the mission analysis [9]. It is assumed that the NavCam acquires images once every 30 minutes and that the onboard EKF is reinitialized with data provided from ground after every orbital manoeuvre. Simulations are conducted using Simulink® R2020a[1]. The simulation environment is based on a 6 degrees of freedom trajectory propagator. Since the GNC and ADCS are developed separately, a representative model of the latter is used for simulation purposes. Furthermore, the Simulink environment is interfaced with Blender®[2] to generate synthetic images in closed-loop during the simulation. Artificial noise is injected into the images to obtain realistic IP performance. An example of the resulting images is reported in Fig. 3. Since the IP uses only global information about the asteroids, a medium-fidelity shape model is used to increase the rendering speed. More details about the simulation environment are given in [14], where preliminary hardware-in-the-loop GNC simulations with representative hardware are also discussed.

The relative level of performance of the different guidance and navigation submodes is illustrated by the performance assessment simulations. Fig. 4 and Fig. 5 report the pointing error and the position estimation error of the different strategies on CRP arc 4b. The latter is the section of CRP arc 4 after the execution of the trajectory correction manoeuvre, which is a challenging phase since the spacecraft gets very close to the system, as seen in Fig. 1b. In general, the pointing error tends

[1] `https://www.mathworks.com/products/simulink.html`. Last accessed: 15/07/2022.
[2] `https://www.blender.org/`. Last accessed: 15/07/2022.

Tab. 4: Description of the GNC simulation categories.

Simulation category	**Description**	**Objective**
Nominal scenarios	Simulations performed in nominal conditions.	To assess the behaviour of the GNC in nominal conditions.
FDIR and nominal events	Simulations of nominal and off-nominal events, like attitude and orbital manoeuvres, sensor faults, etc.	To verify the correct response of the GNC to nominal and off-nominal events.
Performance assessment	Simulations performed on dispersed trajectory arcs and with varying guidance and IP settings.	To assess the performance of the different guidance strategies on dispersed trajectories.
Monte Carlo	Sets of 100 simulations performed on dispersed trajectories.	To assess the robustness of the GNC.

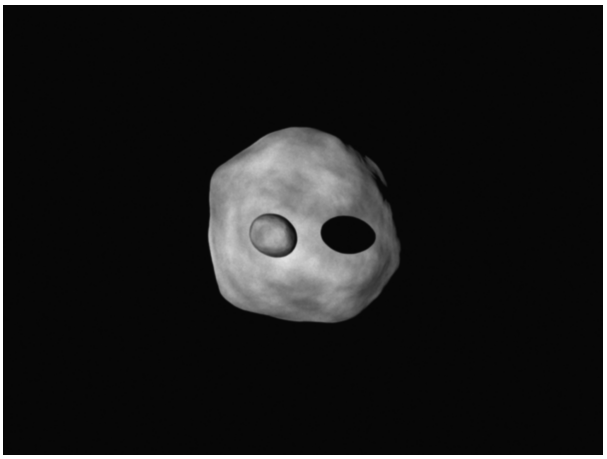

Fig. 3: Example of synthetic image used for the GNC simulations.

to increase as the spacecraft gets closer, as expected. *Predicted* with WCOB and SSWCOB give the lowest error, followed by *Tracking* with WCOB and SSWCOB. For most of the arc, the COB method gives significantly worse results than the other IP techniques, and it recovers only towards the end. This is due to the fact that the phase angle is near 90° at the beginning of the simulation, and it decreases as the spacecraft moves along the arc. In *Reference*, the error is initially in line with the other guidance strategies, but then increases significantly. Indeed, the accuracy of the ephemerides stored onboard inevitably degrades as time passes. The same can be observed from the navigation results in Fig. 5.

The estimation error in *Nav. from EKF* follows a different trend. It increases during the arc and then decreases towards the end. However, since most of the estimation error is concentrated in the direction of the camera boresight, it does not contribute to the pointing error in *Predicted* mode, which remains roughly constant during the arc. This is also confirmed by Fig. 6, where the position estimation error of the EKF is reported in the x, y, and z directions of the SC_NAVCAM frame, together with its expected 3σ bounds. The SC_NAVCAM frame has the origin corresponding to the spacecraft's center of mass, the z-axis aligned with the boresight of the camera, and the x- and y-axes parallel to the image plane, aligned with the horizontal and vertical direction of the image, respectively. As expected, the error in the z direction is significantly larger than the others. Indeed, the CoF measurement only provides information in the image plane, while it is insensitive along the direction of the camera boresight. The estimation error agrees well with the expected standard deviation, except for the x direction when using COB. As discussed in Sec. 4.3, this is due to a bias in the CoF measurement at high phase angles. The WCOB and SSWCOB techniques correct this bias, while the COB does not. This effect reduces along the arc, as the phase angle decreases. Near the end of the arc, after about 4 days, the error and the standard deviation in the z direction significantly decrease when the distance from D1 is low enough to start using lidar measurements.

An example of the application of FDIR logics is reported in Fig. 7. It shows a simulation in which the camera is temporarily turned off after about 2.5 hours, then it is turned back on after another 10 hours. Initially, the system behaves nominally, and the guidance submode immediately switches to *Tracking*, and then to *Predicted*. Similarly, the navigation submode switches to *Nav. from Eph.* and then to *Nav. from EKF*. The highest submodes are not reached immediately because the EKF consistency flag is by default set to 0 at the beginning of each arc. The EKF submode shows that the EKF solution is propagated every 30 seconds and IP data are used every 30 minutes. Lidar measurements are not available because of the distance from the system. As soon as the camera is turned off, the EKF stops using

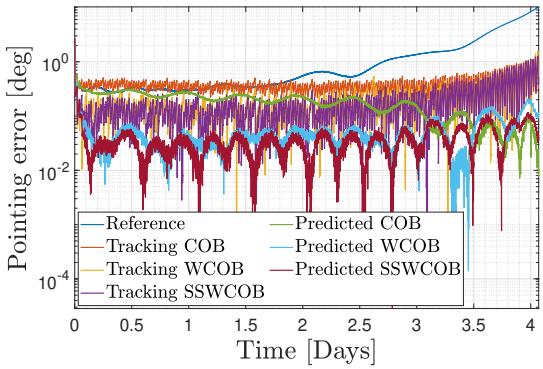

Fig. 4: Pointing error for each combination of guidance and IP modes.

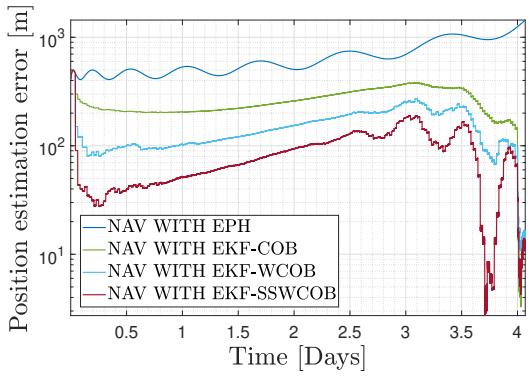

Fig. 5: Position estimation error for each combination of navigation and IP modes.

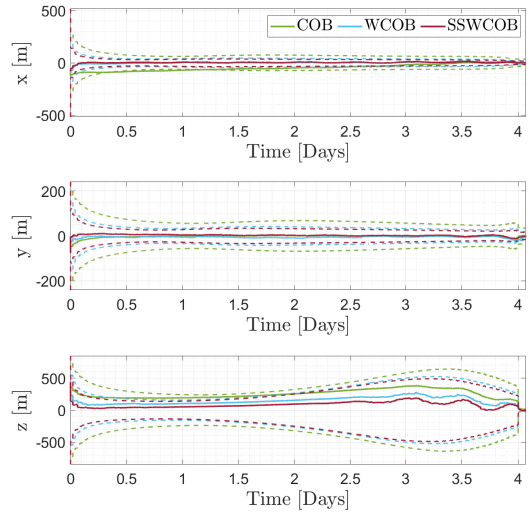

Fig. 6: EKF position estimation error for the different IP techniques. Dashed lines represent the expected 3σ bounds.

measurements. The guidance and navigation submodes initially remain in *Predicted* and *Nav. From EKF*, respectively. This is an intended behaviour, to avoid unnecessary slew manoeuvres in case the camera quickly resumes working. After a predefined amount of time, the guidance submode automatically goes down to *Reference* and the navigation submode to *Nav. From Eph.* These submodes do not require the navigation camera to work, as they rely only on data stored onboard. As soon as the camera is turned back on, all modules resume working as expected.

Finally, the results of the Monte Carlo simulations on FRP arc 1 and CRP arc 1b are reported in Figs. 8 to 13. 100 test cases are considered for each of them. The desired IP mode is set to SSWCOB, while the desired guidance and navigation submodes are *Predicted* and *Nav. From EKF*, respectively. Fig. 9, 10, 12, and 13 show the pointing error and the position estimation error on the two arcs, for each of the test cases, together with the respective requirements. The errors are well below the requirements in most simulations. There are only a couple of cases in CRP arc 1b in which the pointing and navigation errors increase abruptly towards the end of the arc. This is due to the fact that the EKF consistency flag goes to 0, therefore the guidance and navigation submodes automatically switch to *Tracking* and *Nav. From Eph.*, respectively. Furthermore, it can be similarly observed that the navigation error is initially high, then decreases. As discussed before, this is because the EKF consistency flag is initially set to 0, so the initial navigation submode is always *Nav. from Eph.* When the flag is switched to 1, the navigation submode switches to *Nav. From EKF* and the estimation error decreases suddenly. Figs. 9 and 12 show that the pointing error has a periodic behaviour, with phases where it is very low alternating with others where it tends to increase. This is due to the fact that D1 moves along an orbit with a radius of about 10 m around the barycenter of the binary system, and this motion is neglected by the GNC. Finally, Figs. 8 and 11 show in more detail the performance of the onboard EKF. The filter is generally consistent. In FRP arc 1, there is one test case initially outside of the 3σ bounds, but it is then recovered. The performance is also good in CRP arc 1b. It is clear how the estimation error and the standard deviation in the z direction decrease when lidar measurements start being processed by the EKF.

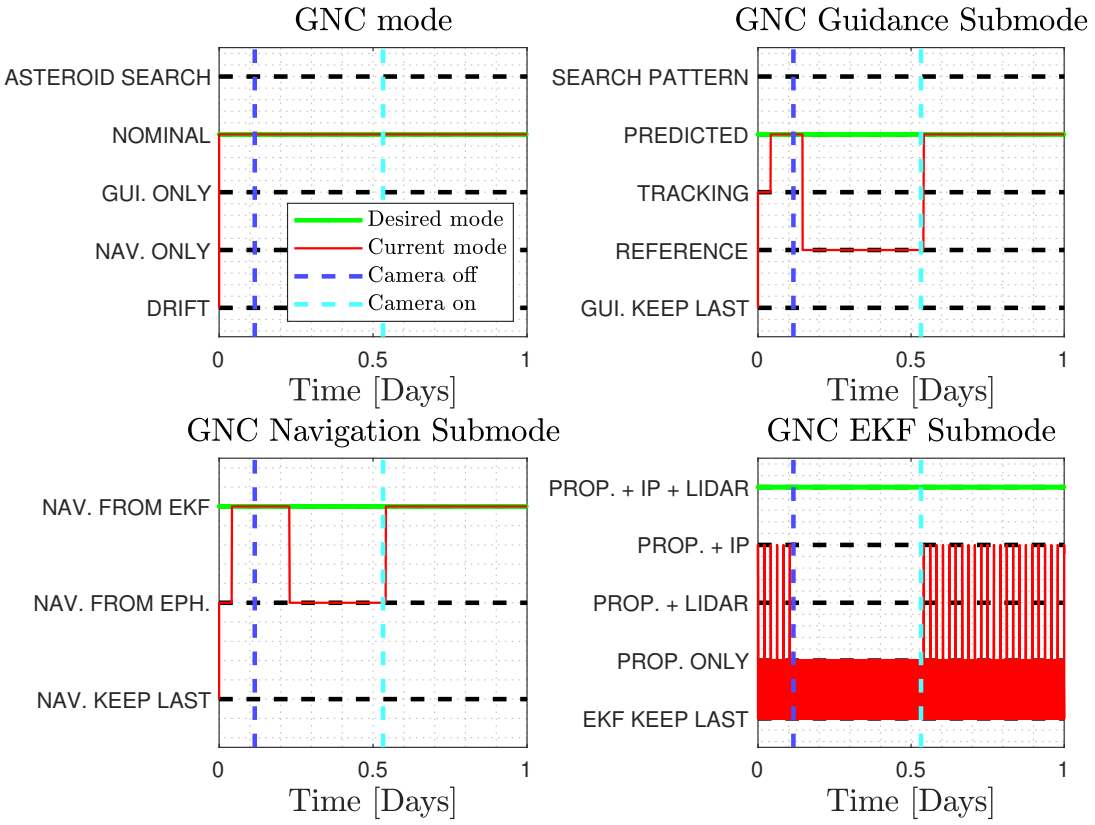

Fig. 7: Response of the different operative modes of the GNC after a simulated navigation camera anomaly. The camera is turned off after about 2.5 hours, then it is turned back on after 10 hours.

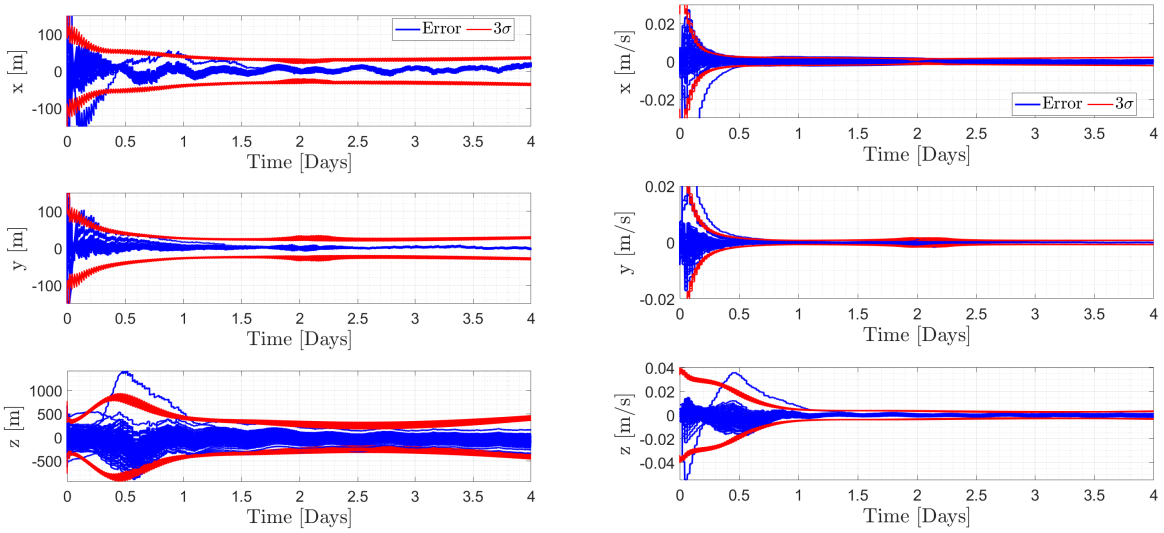

(a) Position error.

(b) Velocity error.

Fig. 8: Performance of the EKF in the Monte Carlo simulation of FRP arc 1.

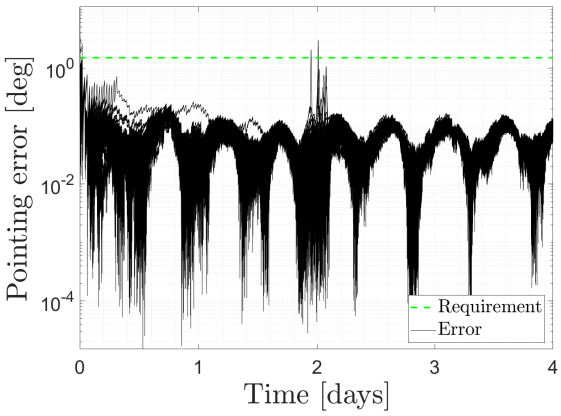

Fig. 9: Pointing error in the Monte Carlo simulation of FRP arc 1.

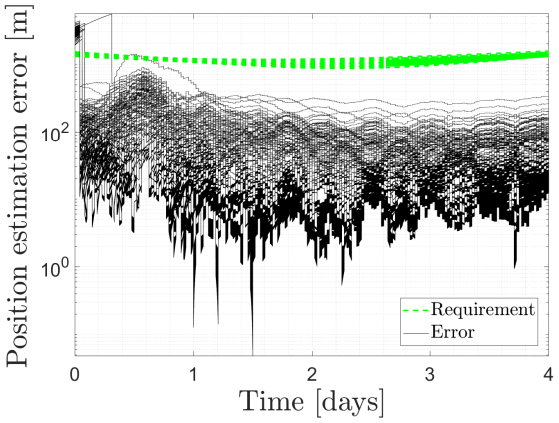

Fig. 10: Position estimation error in the Monte Carlo simulation of FRP arc 1.

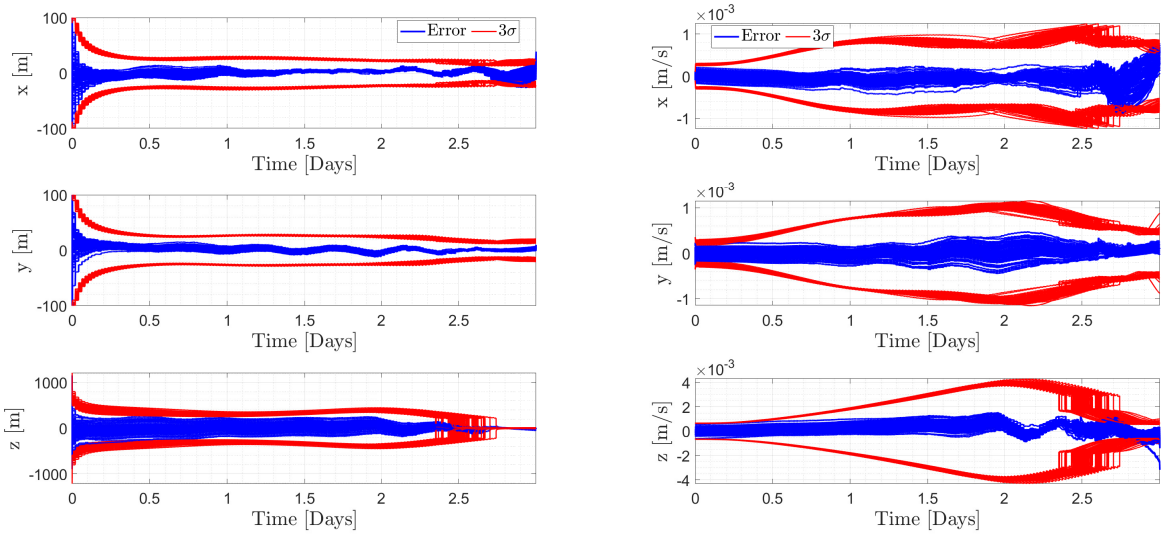

(a) Position error

(b) Velocity error

Fig. 11: Performance of the EKF in the Monte Carlo simulation of CRP arc 1b.

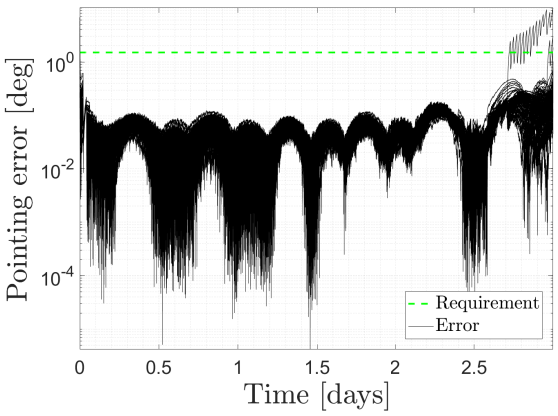

Fig. 12: Pointing error in the Monte Carlo simulation of CRP arc 1b.

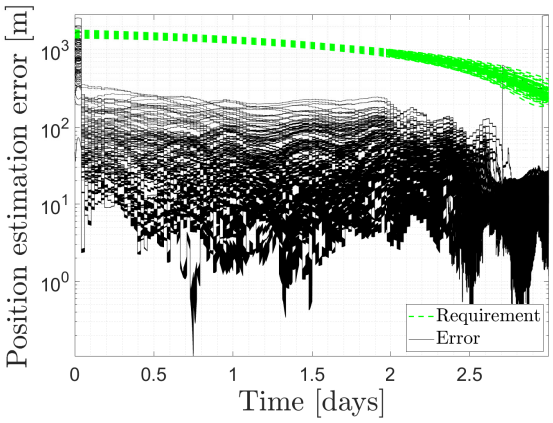

Fig. 13: Position estimation error in the Monte Carlo simulation of CRP arc 1b.

6 Conclusion

This work described in detail the GNC subsystem of the Milani CubeSat. The proposed design proved to be compliant with mission requirements. Thanks to the integration with an innovative IP pipeline, the GNC can autonomously estimate the spacecraft state and point at the desired target. Alternative guidance and navigation strategies have been implemented to increase the robustness of the system. Even if less accurate, they can be used to obtain a pointing and navigation solution in case of anomalies and sensor faults. The GNC can autonomously switch between the different operative modes to obtain the best performance with the available data. This capability has been evaluated by extensive simulations, in which both nominal and off-nominal scenarios have been tested.

Milani completed Phase C with a successful CDR during spring 2022, and has now entered Phase D, during which the onboard software is going to be integrated. The GNC software has been devised to be easily converted to flight code using the autocoding capability of Simulink. Future work will focus on hardware-in-the-loop tests to validate the capability of the GNC and IP to verify mission requirements with images taken by an engineering model of the NavCam.

Acknowledgments

This work is part of the ESA contract No. 4000131925/20/NL/GLC for the mission phases A/B/C/D/E of Milani. The authors would like to acknowledge the support received by the whole Milani consortium, which is lead by Tyvak International. M.P and F.T would like to acknowledge the funding received from the European Union's Horizon 2020 research and innovation programme under the Marie Skłodowska-Curie grant agreement No 813644.

Bibliography

[1] A F Cheng, A S Rivkin, P Michel, J Atchison, O Barnouin, L Benner, N L Chabot, C Ernst, E G Fahnestock, M Kueppers, et al. AIDA DART asteroid deflection test: Planetary defense and science objectives. *Planetary and Space Science*, 157:104–115, 2018.

[2] Andrew S Rivkin, Nancy L Chabot, Angela M Stickle, Cristina A Thomas, Derek C Richardson, Olivier Barnouin, Eugene G Fahnestock, Carolyn M Ernst, Andrew F Cheng, Steven Chesley, et al. The double asteroid redirection test (DART): planetary defense investigations and requirements. *The Planetary Science Journal*, 2(5):173, 2021.

[3] Patrick Michel, Michael Küppers, and Ian Carnelli. The Hera mission: European component of the ESA-NASA AIDA mission to a binary asteroid. *42nd COSPAR Scientific Assembly*, 42:B1–1, 2018.

[4] F Ferrari, V Franzese, M Pugliatti, C Giordano, and F Topputo. Preliminary mission profile of Hera's Milani CubeSat. *Advances in Space Research*, 67(6):2010–2029, 2021.

[5] Ö Karatekin, E Le Bras, A Herique, P Tortora, B Ritter, M Scoubeau, V M Moreno, et al. Juventas Cubesat for the Hera mision. In *15th European Planetary Science Congress*, 2021.

[6] M Pugliatti, A Rizza, F Piccolo, V Franzese, C Bottiglieri, C Giordano, F Ferrari, and F Topputo. The Milani mission: overview and architecture of the optical-based GNC system. In *AIAA Scitech 2022 Forum*, 2022.

[7] M Pugliatti, V Franzese, and F Topputo. Data-Driven Image Processing for Onboard Optical Navigation Around a Binary Asteroid. *Journal of Spacecraft and Rockets*, 59(3):943–959, 2022.

[8] M Pugliatti, V Franzese, A Rizza, F Piccolo, C Bottiglieri, C Giordano, F Ferrari, and F Topputo. Design of the on-board image processing of the Milani mission. In *44th AAS Guidance, Navigation and Control Conference*, 2022.

[9] C Bottiglieri, F Piccolo, A Rizza, M Pugliatti, V Franzese, C Giordano, F Ferrari, and F Topputo. Mission Analysis and Navigation Assessment for Hera's Milani CubeSat. In *4S Symposium 2022*, 2022.

[10] F Ferrari, V Franzese, M Pugliatti, C Giordano, and F Topputo. Trajectory Options for Hera's Milani CubeSat Around (65803) Didymos. *The Journal of the Astronautical Sciences*, 68(4):973–994, 2021.

[11] T Kohout, A Näsilä, T Tikka, M Granvik, A Kestilä, A Penttilä, J Kuhno, K Muinonen, K Viherkanto, and E Kallio. Feasibility of asteroid exploration using CubeSats—ASPECT case study. *Advances in Space Research*, 62(8):2239–2244, 2018.

[12] F Dirri, E Palomba, A Longobardo, D Biondi, A Boccaccini, A Galiano, E Zampetti, B Saggin,

D Scaccabarozzi, and J Martin-Torres. VISTA Instrument: A PCM-Based sensor for organics and volatiles characterization by using thermogravimetric technique. In *2018 5th IEEE International Workshop on Metrology for AeroSpace*, 2018.

[13] J R Carpenter and C N D'Souza. Navigation filter best practices. Technical report, 2018.

[14] A Rizza, F Piccolo, M Pugliatti, P Panicucci, and F Topputo. Hardware-in-the-loop validation for Milani CubeSat vision-based GNC. In *73rd International Astronautical Congress*, 2022.